Anal Bioanal Chem (2010) 397:2109–2116
DOI 10.1007/s00216-010-3775-8

ORIGINAL PAPER

Synchrotron microangiography studies of angiogenesis in mice with microemulsions and gold nanoparticles

Chia-Chi Chien · C. H. Wang · C. L. Wang · E. R. Li · K. H. Lee · Y. Hwu · Chien-Yi Lin · Shing-Jyh Chang · C. S. Yang · Cyril Petibois · G. Margaritondo

Received: 7 February 2010 / Revised: 17 April 2010 / Accepted: 22 April 2010 / Published online: 6 June 2010

Abstract We present an effective solution for the problem of contrast enhancement in phase-contrast microangiography, with the specific objective of visualising small (<8 μm) vessels in tumor-related microangiogenesis. Different hydrophilic and hydrophobic contrast agents were explored in this context. We found that an emulsified version of the hydrophobic contrast agents Lipiodol® provides the best contrast and minimal distortion of the circulation and vessel structure. Such emulsions are reasonably biocompatible and, with sizes of 0±0.8 μm, sufficient to diffuse to the smallest vessel and still provide reasonable contrast. We also explored the use of Au nanoparticle colloids that could be used not only to enhance contrast but also for interesting applications in nanomedicine. Both the Lipiodol microemulsions and Au nanoparticle colloids can be conjugated with medicines or cell specific labeling agents and their small size can allow the study of the diffusion of contrast agents through the vessel leakage. This enables direct imaging of drug delivery which is important for cancer treatment.

Keywords Microradiology · Microangiography · Angiogenesis · Micro-emulsion · Gold nanoparticles · Contrast agent

C.-C. Chien · C. H. Wang · C. L. Wang · E. R. Li · K. H. Lee · Y. Hwu (✉)
Institute of Physics, Academia Sinica,
Nankang,
Taipei 115, Taiwan, China
e-mail: phhwu@sinica.edu.tw

C.-C. Chien · Y. Hwu
Department of Engineering and System Science,
National Tsing Hua University,
Hsinchu 300, Taiwan, China

Y. Hwu
Institute of Optoelectronic Sciences,
National Taiwan Ocean University,
Keelung 202, Taiwan, China

C.-Y. Lin · S.-J. Chang
Hsinchu Mackay Memorial Hospital,
Hsinchu 300, Taiwan, China

C. S. Yang
Center for Nanomedicine, National Health Research Institutes,
Miaoli 350, Taiwan, China

C. Petibois
Université de Bordeaux 2,
CNRS UMR 5248, CBMN, B8, Avenue des faculties,
33405 Talence-Cedex, France

G. Margaritondo
Ecole Polytechnique Fédérale de Lausanne (EPFL),
1015 Lausanne, Switzerland

Introduction

Microradiology based on coherent synchrotron X-rays can provide the required lateral and time resolution for angiography studies of microangiogenesis [1–3]. With bright unmonochromatized synchrotron X-rays, the image taking is fast enough to limit the motion blurring and to allow high resolution observation of the smallest vessels in live animals [4]. However, finding a suitable contrast agent is not a trivial problem since those used in conventional radiology do not work well for phase-contrast microangiography with high lateral resolution. Most certified contrast agents for clinical use are nonionic, such as Iomeprol®, Imeron®, and Hexabrix®, whose fast diffusion rate limits their application to image small capillaries (<20 μm) in small animals [5–9]. Therefore, they are not

satisfactory for the purpose of enhancing the weak contrast of the microvessels with respect to the surrounding tissues to study tumor angiogenesis with whole tumor profiling in vivo without losing important information of the three-dimensional structure of the smallest vessels.

We solved this problem after testing different hydrophilic and hydrophobic contrast agents. One of the good candidate of such solution is the emulsification of a hydrophobic and otherwise viscous contrast agent, Lipiodol®; this enabled us to reach not only a lateral resolution ~2 μm and a time resolution ~1 ms, but also to detect tumor microvessels as small as 7–8 μm in live mice. Nanoparticle systems with good colloidal stability and high enough X-ray absorption can perform a similar function.

These results are quite important for microangiogenesis studies—and for many similar issues in biomedical research. Important syndromes, notably vascular diseases and cancer, are related to the growth of small vessels and to changes in their fine morphology [2, 3]. In tumor growth, permeable small vessels are believed to provide nutrients to tumor cells [10]. Angiogenesis control can thus be an effective way to fight cancer [11, 12]. But the implementation of new therapies requires a detailed knowledge of angiogenesis on a scale <8 μm with the use of suitable imaging techniques.

Widely used approaches such as magnetic resonance imaging (MRI) [13, 14], single photon-emission computed tomography (SPECT), positron emission tomography (PET) [15], ultrasonography [16, 17], optical coherent tomography (OCT) [18, 19], and computed tomography (CT) [20–24] suffer from insufficient lateral resolution. The permeability of fluorescent macromolecules can be observed with the intravital imaging method [25–28]—but this approach is limited to near-surface regions due to the low penetration of visible light. Post-mortem examinations using other types of microscopies, such as optical, electron, or infrared [29–31], cannot study time-evolving phenomena except with a large number of killed animals. The fast circulation rate in mice [32], with a velocity in the pulmonary artery as high 35 cm/s in the systolic phase [33], complicates the problem.

We show here that synchrotron microradiology [1, 34] can solve this problem if a suitable answer is found for the question of contrast enhancement. Thanks to the adjustable image acquisition geometry and the high coherence of synchrotron sources, phase (or refractive index) contrast is very effective in enhancing features with low absorption contrast [35] such as blood vessels [4, 36–40]. The high source brightness makes it possible to achieve fast imaging at the microsecond level with approximately micrometer level lateral resolution [41, 42]. The fast image taking is essential since small movements even for deep anesthetized animals would cause motion blur and jeopardize the detection of <10 μm vessels.

In our search for a suitable contrast agent for synchrotron microangiography, we found that viscosity and solubility are the most relevant factors. Viscous hydrophobic agents are resistant to dilution and therefore easier to detect. However, such agents do not flow smoothly and are likely to deform small vessels affecting size and position measurements.

Aqueous hydrophilic agents are quickly diluted in the blood stream, making it difficult to detect in real time their circulation. On the positive side, such agents have limited adverse effects on the vascular structure as well as the health of animals. It is also possible to use these agents to study the diffusion through the leaky vessels.

Based on these observations, we successfully tested a new type of contrast agent by emulsifying viscous hydrophobic Lipiodol®. The result is better microvessel detectability than with hydrophilic agents and a natural circulation suitable for real-time microradiology. With this agent, we achieved performances similar to Lipiodol in the detection of small vessels. And we were able to observe its diffusion through small vessels.

Finally, we also explored the use of aqueous PEG-Au nanoparticle colloids [43]. They behave like hydrophilic contrast but provide additional functions. The small nanoparticle size and the leaky nature of microvessels lead to highly selective localization at tumor sites by the EPR (enhanced retention and permeation) effect. After injecting 35 μl of PEG-Au solution (55 mg/ml) into a mouse tail vein, we found the accumulation to start within seconds (120 s) and the differential concentration to increase for at least 12 h [44]. This made it possible to highlight small vessels of 10 μm size sufficient for microradiology.

Note that both types of agents, microemulsions and nanoparticle colloids can be used as drug carriers [45–47]. If combined with suitable molecules for treatment, our imaging strategy could thus increase the probability of coordinated application to effective cancer diagnosis and nanomedicine delivery. Furthermore, the possibility to study microvascular structures on a very small scale could by itself open new door to the study of microangiogensis in full three dimensions with high lateral and time resolution.

Experimental

All procedures involving animals were approved by Academia Sinica Institutional Animal Care and Utilization Committee (AS IACUC). BALB/cByJNarl mice were provided by National Laboratory Animal Center, Taiwan. All mice were housed in individual ventilated cages (five per cage) with wood chip bedding and kept at 24±2 °C with a humidity of 40–70% and a 12-h light/dark cycle. The tests were performed on 5-weeks old Balb/c mice after injection of the highly metastatic cancer cell strain CT-26,

suitable for tumor angiogenesis studies. CT-26 cells (1×10^6) in 10 μl RPMI-1640 medium were subcutaneous-injected in the left thigh region. Tumor volume was estimated by adopting a formula $v = 0.5 \times a \times b^2$, where a and b are the smallest and the largest diameters, respectively. Treatment of tumors was started after about 7 days, for example as shown in Fig. 1, when they reached a size of 100 to 120 mm^3 and after 26 days when they reached a size of 1,000 to 1,200 mm^3.

The explored contrast agents included commercial Hexabrix® (Guerbet, Aulnay-sous-Bios, France) and Lipiodol® (Guerbet, Aulnay-sous-Bios, France). Typically, 70 μl of Hexabrix® (320 mg/ml of iodine) or 40 μl (480 mg/ml of iodine) Lipiodol® were injected via thigh artery.

In the case of emulsified Lipiodol®, the iodine concentration was ~240 mg/ml and a volume of 50 μl was injected. The emulsified Lipiodol® was prepared by mixing two solutions: solution A, which is 0.1 ml of span-80 mixed with 1 ml of Lipiodol®, and solution B, which is 0.6 ml Tween-20 mixed with 3 ml of phosphate buffer solution. By adding the hydrophobic solution A with the aqueous solution B in a 2:1 ratio, and stirring for 8 h, the emulsified solution is formed with small droplets of size in the μm range. The two surfactants, Span-80 and Tween-20, are polysorbate emulsifiers widely used in food additive and cosmetics. These emulsifiers interface Lipiodol and water and stabilize and suspended the encapsulated Lipiodol droplets. Before injection, this emulsified Lipiodol® solution was sonicated for 15 min to ensure a homogenized suspension.

In a separate series of tests, we injected ~35 μl of a colloidal solution of PEG-Au nanoparticles synthesized by a special X-ray irradiation method [36], whose concentration was increased to 36 mg/ml of Au with several rounds of centrifuge separation and cleaning.

PE-05 catheters (BB31695, Scientific Commodities, Inc., I.D.: 0.2 mm, O.D.: 0.36 mm) were used to inject the contrast agents. The catheter was placed under anesthesia induced by intramuscular injection of 10 μl of Zoletil 50 (50 mg/kg; Virbac Laboratories, Carros, France) per mouse (weight ~20–25 g). The anterior tight skin was incised along a 1-cm^2 circle and after a sharp dissection, the catheter was inserted into the femoral artery and secured by a 6-0 nylon ligature. With the mouse in the imaging position, one of the aforementioned contrast agents was injected at a 0.5 μl/s rate. During imaging, the mice were kept under anesthesia using 1% isoflurane in oxygen.

Microradiology was implemented with unmonochromatized (white) synchrotron X-rays emitted by the 01-A beamline wavelength shifter of the National Synchrotron Radiation Research Center (Taiwan) [48]. The photon energy ranged from 4 keV to 30 keV with a peak intensity at energy ~12 keV and the beam current was kept constant at 300 mA with the top-up operation mode. To obtain 3×3 mm images, the X-rays were first converted to visible light by a $CdWO_4$ single crystal scintillator and then captured by an optical microscope with a CCD camera (Andor, 1,000×1,000 pixels). The radiation dose was reduced by attenuating the emitted X-ray beam with two pieces of 550 μm single crystalline silicon wafers placed before the animal.

The exposure time was ~100 ms and the distance between the sample and the scintillator was ~5 cm; a ×2, ×5, or ×10 lens in the optical microscope was used to obtain the desired field of view. The size of each pixel in the final image taken with the ×5 lens was ~2.4×2.4 μm^2.

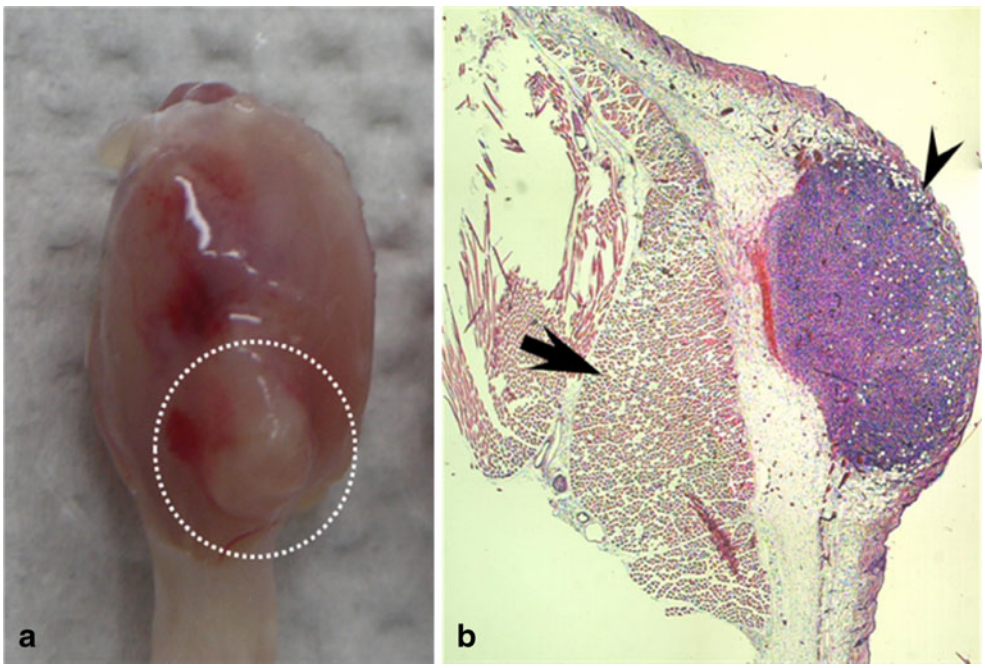

Fig. 1 Photograph of a typical tumor grown at mouse thigh to a size ~100–120 mm^3 7 days after the plantation which is marked by a *white circle* on the leg in (**a**). Tumor pathological image of a section of the whole tumor is shown in (**b**), the developed tumor is stained in *purple color* in the subcutaneous tissue. The *pink color* is the muscle

Results and discussion

The preliminary tests with the commercial Hexabrix® and Lipiodol® as contrast agent for microangiography were not satisfactory. Specifically, hydrophilic Hexabrix® diffused immediately by flowing through the vessels, especially in the tumor site. The more Hexabrix® was injected, the darker became the background in the surrounding tissue, making the vessels in the tumor site difficult to detect. This can be seen in Fig. 2 b–d that shows radiographs taken at a normal tissue area, marked by the square in Fig. 2a 62.1, 89.4, and 102.6 seconds after injection of the Hexabrix. The smallest detectable vessel size in this case was ~24 μm (in the femoral artery site) at the normal tissue area. The arrow heads marked areas showing significant diffusion of contrast agent out of the vessels.

The strong Hexabrix® diffusion is observed not only in the normal vessels but also in the tumor area. In the tumor area, marked by letter T at the left part of Fig. 2a, we can only detect the whole area become darker with respect to surrounding tissue, where the boundary is marked by an arrow head and to that before injection. The parallel vessel structure in muscle site (marked by letter N) also showed strongly diffused Hexabrix® (marked by arrows). Driven by the concentration gradient, Hexabrix® diffused to the interstitial tissues and the abnormal vessels with intercellular openings and transvascular holes [11]. This causes it to be rapidly diluted by blood before producing sufficient contrast for small vessels. The diffusion smears even the sharp phase-contrast edges observed with no contrast agent [4].

Hydrophobic and viscous Lipiodol®, seldom used for vessel imaging, behaved quite differently. Clinicians use this agent to image lymph or ovary and for vascular embolization in liver cancer. Likewise, we observed Lipiodol® flowing to mouse lungs and plugging the alveoli capillaries (data not show). We also observed that in tumor sites the slow flowing agent enlarged the vessels and jeopardized the accuracy of vessel size estimates. On the other hand, it did not rapidly diffuse and this enabled us to observe its presence in small vessel. In Fig. 3, for example, the smallest detectable vessel size in this set of microradiographs is ~14.4 μm (marked by the arrow head in Fig 3b).

We also see that the hydrophobicity of Lipiodol® leads to the creation of small droplet (marked by the arrow in Fig. 3b and c), particularly for microscopic vessels, that complicate the image analysis and tracing [3]. These problems led us to the idea of using an emulsified version of Lipiodol® that is not as easily diluted as Hexabrix® but flows much better than Lipiodol®. By directly monitoring the flow of emulsified microspheres, we could image very small vessels at the tumor site (Fig. 4, 7 days after tumor injection), even for large and thick tumors (Fig. 5, 26 days). The smallest detected vessel size was ~7.6 μm. The total amount of injected emulsified Lipiodol® was less than one-half of that of standard Lipiodol®.

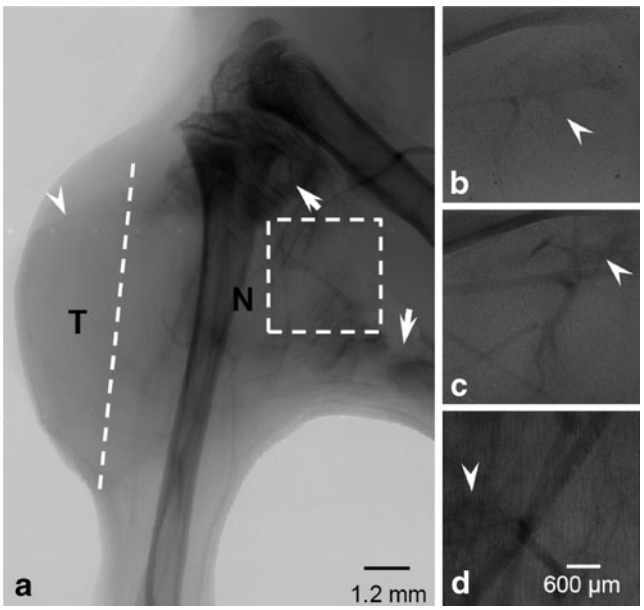

Fig. 2 Microradiographs of vessels in different popliteal regions after a 70 μl Hexabrix® injection: **a** entire leg, **b**, **c**, and **d**: zoom-in images of the area marked in **a** taken 62.1, 89.4, and 102.6 s after injection. The lack of clear microvessel structure at the tumor site in **a** is attributed to the strong diffusion of the contrast agent. At normal tissue areas (such as that marked by *N*), the *arrows* in **a** and the *arrowheads* in **b**–**d** indicate areas showing significant diffusion of the contrast agent

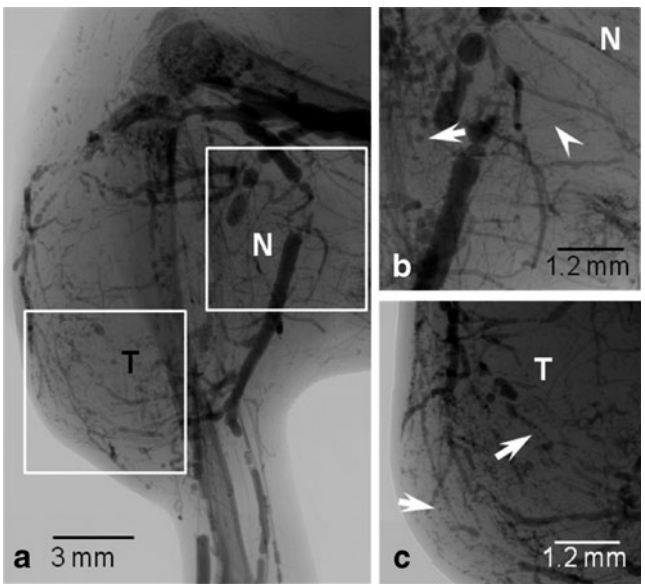

Fig. 3 Microradiographs of vessels in different popliteal region after a 70 μl Lipiodol® injection: **a** entire leg, **b** femur site (*N*), and **c** tumor site (*T*). *Arrows* marked vessels of smallest size and the *arrowheads* marked the small emulsion droplets

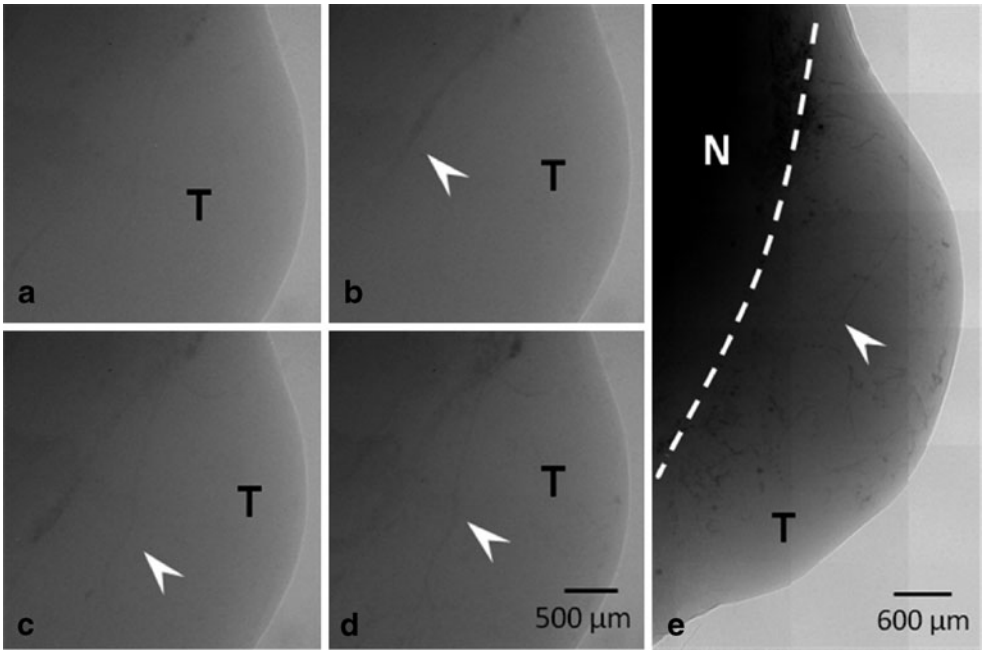

Fig. 4 Microradiographs (taken with a ×2 lens) of tumor vessels after a 40 µl emulsified Lipiodol® injection: **a** 20.1, **b** 38.7, **c** 50.7, and **d** 108.6 s after injection; **e** image taken with a ×5 lens. *Arrowheads* marked one specific vessel outlined by the flow of the contrast agent

More specifically, Fig. 4a–d show images taken 20.1, 38.7, 50.7, and 108.6 s after the emulsified Lipiodol® injection. The slow flow of the contrast agent progressively outlines the vessels, as marked by arrowheads, in the tumor. Note that images taken with low resolution (×2 lens, Fig. 4a–d) do not show clear capillary vessels whereas they are readily seen in the higher-resolution picture (×5 lens, Fig. 4e). This is reasonable since the size of emulsified Lipiodol® particles is of a few micrometers. The typical optical image of such emulsion shown in Fig. 6 indicates that the average droplet size is ~2 µm. Such a small size guarantees that they flow to the smallest vessel with limited perturbation of the vascular structures. Fast image taking was again confirmed to be important to avoid excessive

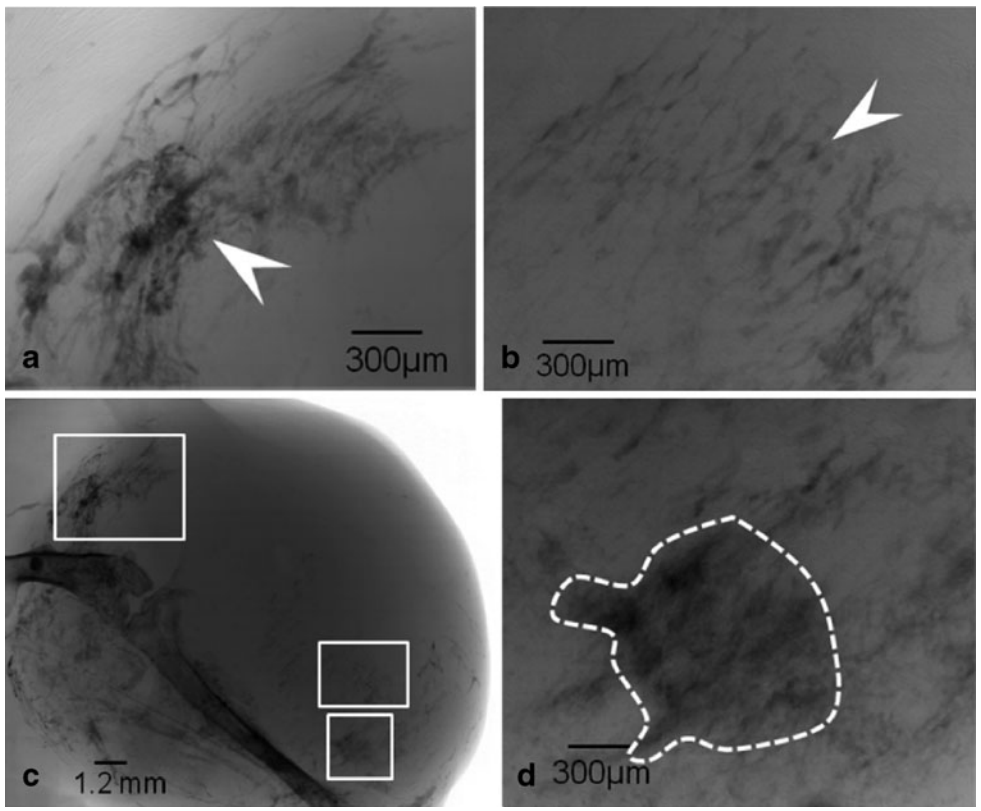

Fig. 5 Microradiographs with contrast enhanced by emulsified Lipiodol® of vessels in a 26 days tumor: **a**, **b** abnormal vessel structure, **c** whole leg image, **d** blood pool. *Arrowheads* in **a** and **b** marked the microvessel areas of tumor angiogenesis. Blood pool outlined in **d** shows no clear vessel structure

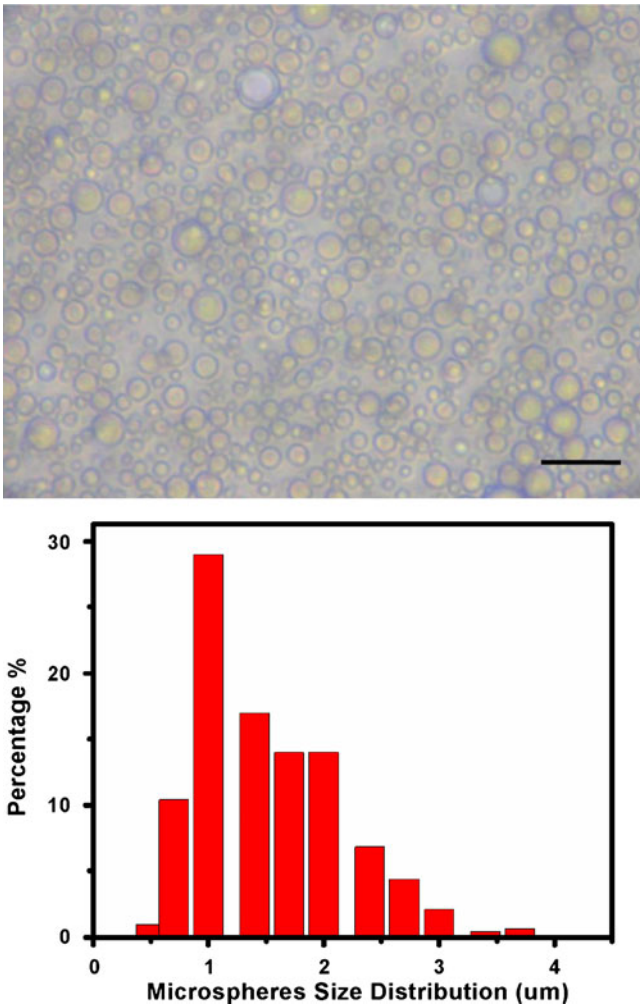

Fig. 6 Optical micrograph of the emulsified Lipiodol® dispersed on a slide surface. *Scale bar* 10 μm. The size distribution is estimated from a number of similar images

motion blur: for example, this prevented us to further improve the image by using a ×20 lens.

Figure 5 shows images with emulsified Lipiodol in mouse tumor area taken 26 days after tumor planting and reveal the abnormal vessel structure. This is particularly clear in the whole leg picture of Fig. 5c. Figure 5a and b show a vessel microstructure, marked by arrow heads in the close vicinity of the tumor site, clearly resulted from the tumor microangiogenesis. We also identified areas, such as that marked in Fig. 5d, as blood pools which show no clear vessel structure. Such image implies that the irregular vessel structure allows the emulsified hydrophobic Lipiodol droplets diffusing out of the vessels to the interstitial tissue.

Finally, we would like to present results for PEG-Au nanoparticles selectively bound because of the EPR effect. The aforementioned new colloidal synthesis method by X-ray irradiation [49, 50] yielded excellent stability and biocompatibility plus high concentration. An aqueous colloid with ~36 mg/ml of PEG-Au with an average Au core size ~7± 2 nm [51] was administrated to mice without any adversary effects.

The PEG coating increased the duration of the presence of nanoparticle in the blood circulation enhancing the flexibility of the microradiology analysis [52]. In fact, the images of Fig. 7 show that the colloid is effective as a contrast agent for a longer time than Hexabrix®. Figure 7a, for example, clearly reveals the artery (arrow heads) and the veins (arrow). However, the hydrophilic nature of the nanoparticle colloid prevents it from imaging microvessels as effectively as emulsified Lipiodol (Fig. 7c). The smallest detectable vessel is in fact >40 μm due to rapid dilution in the blood stream.

Although emulsified hydrophobic agent are inexpensive and easy to make, it is well known that one of the most important application of microemulsions and nanoparticle colloid is not only to enhance the contrast but also to obtain other functions such as specific cancer targeting, diagnosis, and radiotherapy [41, 53–56]. The PEG-Au nanoparticles can be easily conjugated with cancer drugs such as TNF-α (tumor necrosis factor-alpha) [45] or doxorubicin [46] and it is not difficult to encapsulate drugs with microemulsions [47], either. Similar imaging approaches can also be applied to other type of nanoparticles [57–59] and delivery system like liposome, micelles, or microspheres as long as high X-ray contrast materials can also be incorporated at the same time.

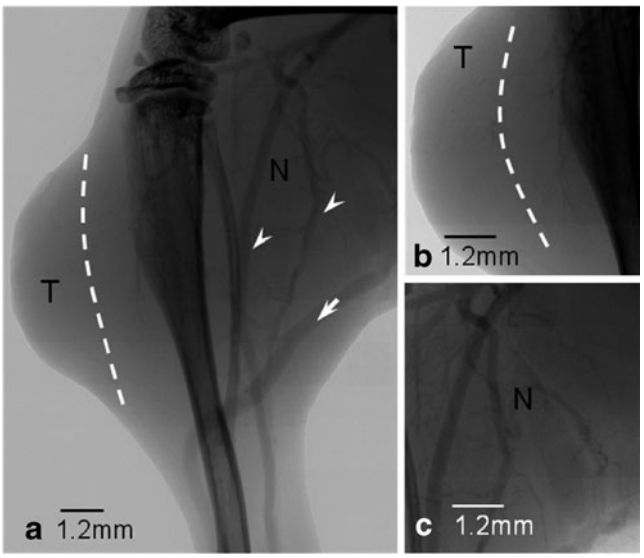

Fig. 7 Photographs (taken with a ×5 lens) of vessels in different popliteal region after a 35 μl of 36 mg/ml PEG-Au nanoparticle colloid injection: **a** entire leg, **b** tumor site; **c** femur site. Although small vessels are not clearly imaged due to the diffusion of small size of PEG-Au nanoparticles, the contrast is sufficient to see clear vessel structures without apparent distortion of the vessel diameter. *Arrowheads* marked, for example, the artery and *arrowheads* marked the vein

Conclusion

In this work, we demonstrated a practical solution for the problem of contrast enhancement in phase-contrast micro-angiography by emulsifying a hydrophobic and otherwise viscous contrast agent. We were thus able to detect vessels as small as ~7–8 μm, thanks in particular to the short image taking time and limited motion blurring. We also explored the use of colloidal PEG-Au for contrast with mildly positive results compensated by the potential use of nano-particles for diagnosis and therapy.

Acknowledgments This work is supported by National Science and Technology Program for Nanoscience and Nanotechnology, the Thematic Research Project of Academia Sinica, the Biomedical Nano-Imaging Core Facility at National Synchrotron Radiation Research Center (Taiwan), the Blonc Project of ANR-NSC (French National Research Agency and Taiwan National Science Council, the Center for Biomedical Imaging (CIBM) in Lausanne, partially funded by the Leenaards and Jeantet foundations and by the Swiss Fonds National de la Recherche Scientifique and by the EPFL.

References

1. Hwu Y, Hsieh HH, Lu MJ, Tsai WL, Lin HM, Goh WC, Lai B, Je JH, Kim CK, Noh DY, Youn HS, Tromba G, Margaritondo G (1999) Coherence-enhanced synchrotron radiology, refraction vs. diffraction mechanisms. J Appl Phys 86:4613–4618
2. Khurana R, Simons M, Martin JF, Zachary IC (2005) Role of angiogenesis in cardiovascular disease—a critical appraisal. Circulation 112:1813–1824
3. Savai R, Langheinrich AC, Schermuly RT, Pullamsetti SS, Dumitrascu R, Traupe H, Rau WS, Seeger W, Grimminger F, Banat GA (2009) Evaluation of angiogenesis using micro-computed tomography in a xenograft mouse model of lung cancer. Neoplasia 11(1):48–56
4. Hwu Y, Tsai WL, Je JH, Seol SK, Kim B, Groso A, Margaritondo G, Lee KH, Seong JK (2004) Synchrotron microangiography with no contrast agent. Phys Med Biol 49:501–508
5. Tokiya R, Umetani K, Imai S, Yamashita T, Hiratsuka J, Imajo Y (2004) Observation of microvasculatures in athymic nude rat transplanted tumor using synchrotron radiation microangiography system. Acad Radiol 11:1039–1046
6. Schwenke DO, Pearson JT, Umetani K, Kangawa K, Shirai M (2007) Imaging of the pulmonary circulation in the closed-chest rat using synchrotron radiation microangiography. J Appl Physiol 102:787–793
7. Morishita A, Kondoh T, Sakurai T, Ikeda M, Bhattacharjee AK, Nakajima S, Kohmura E, Yokono K, Umetani K (2006) Quantification of distension in rat cerebral perforating arteries. NeuroReport 17:1549–1553
8. Imazuru T, Matsushita S, Hyodo K, Tokunaga C, Kanemoto S, Enomoto Y, Watanabe Y, Hiramatsu Y, Sakakibara Y (2009) Erythropoietin enhances arterioles more significantly than it does capillaries in an infarcted rat heart model. Int Heart J 50:801–810
9. Schwenke DO, Pearson JT, Kangawa K, Umetani K, Shirai M (2008) Changes in macrovessel pulmonary blood flow distribution following chronic hypoxia: assessed using synchrotron radiation microangiography. J Appl Physiol 104:88–96
10. Carmeliet P, Jain RK (2000) Angiogenesis in cancer and other diseases. Nature 407:249–257
11. Hashizume H, Baluk P, Morikawa S, McLean JW, Thurston G, Roberge S, Jain RK, McDonald DM (2000) Openings between defective endothelial cells explain tumor vessel leakiness. Am J Pathol 156:1363–1380
12. McDonald DM, Baluk P (2002) Significance of blood vessel leakiness in cancer. Cancer Res 62:5381–5385
13. Bolan PJ, Yacoub E, Garwood M, Ugurbil K, Harel N (2006) In vivo micro-MRI of intracortical neurovasculature. Neuroimage 32:62–69
14. Cuenod CA, Fournier L, Balvay D, Guinebretiere JM (2006) Tumor angiogenesis: pathophysiology and implications for contrast-enhanced MRI and CT assessment. Abdom Imaging 31:188–193
15. Gambhir SS (2002) Molecular imaging of cancer with positron emission tomography. Nat Rev Cancer 2:683–693
16. Ogura O, Takebayashi Y, Sameshima T, Maeda S, Yamada K, Hata K, Akiba S, Aikour T (2001) Preoperative assessment of vascularity by color Doppler ultrasonography in human rectal carcinoma. Dis Colon Rectum 44:538–546
17. Park KS, Choi BI, Won HJ, Seo JB, Kim SH, Kim TK, Han JK, Yeon KM (1998) Intratumoral vascularity of experimentally induced VX2 carcinoma: comparison of color Doppler sonography, power Doppler sonography, and microangiography. Invest Radiol 33(1):39–44
18. Gambichler T, Moussa G, Sand M, Sand D, Altmeyer P, Hoffmann KJ (2005) Applications of optical coherence tomography in dermatology. Dermatol Sci 40(2):85–94
19. An L, Wang RK (2008) In vivo volumetric imaging of vascular perfusion within human retina and choroids with optical micro-angiography. Opt Express 16(15):11438–11452
20. Lee TY, Purdie TG, Stewart EQ (2003) CT imaging of angiogenesis. J Nucl Med 47:171–187
21. Weissleder R (2002) Scaling down imaging: molecular mapping of cancer in mice. Nat Rev Cancer 2:11–18
22. Goh V, Padhani AR, Rasheed S (2007) Functional imaging of colorectal cancer angiogenesis. Lancet Oncol 8:245–255
23. McDonald DM, Choyke PL (2003) Imaging of angiogenesis: from microscope to clinic. Nat Med 9:713–725
24. Rabin O, Manuel Perez J, Grimm J, Wojtkiewicz G, Weissleder R (2006) An X-ray computed tomography imaging agent based on long-circulating bismuth sulphide nanoparticles. Nat Mater 5:118–122
25. Jain RK, Munn LL, Fukumura D (2002) Dissecting tumour pathophysiology using intravital microscopy. Nat Rev Cancer 2:266–276
26. Mulder WJ, Castermans K, van Beijnum JR, Oude Egbrink MG, Chin PT, Fayad ZA, Löwik CW, Kaijzel EL, Que I, Storm G, Strijkers GJ, Griffioen AW, Nicolay K (2009) Molecular imaging of tumor angiogenesis using alphavbeta3-integrin targeted multi-modal quantum dots. Angiogenesis 12:17–24
27. Walls JR, Coultas L, Rossant J, Henkelman RM (2008) Three-dimensional analysis of vascular development in the mouse embryo. PLoS ONE 3:e2853
28. Fukumura D, Jain RK (2008) Imaging angiogenesis and the microenvironment. APMIS 116:695–715
29. Petibois C, Piccinini M, Cestelli-Guidi M, Déléris G, Marcelli A (2009) A bright future for synchrotron imaging. Nat Photonics 3:179
30. Belbachir K, Noreen R, Gouspillou G, Petibois C (2009) Collagen types analysis and differentiation by FTIR spectroscopy. Anal Bioanal Chem 385:829–837
31. Wehbe K, Pinneau R, Moenner M, Déléris G, Petibois C (2008) FT-IR spectral imaging of protein content changes in blood vessels during tumor growth. Anal Bioanal Chem 392:129–135
32. Yeh CK, Chen JJ, Li ML, Luh JJ, Chen JJ (2009) In vivo imaging of blood flow in the mouse Achilles tendon using high-frequency ultrasound. Ultrasonics 49:226–230

33. Parzya E, Miraux S, Franconi J, Thiaudière E (2009) In vivo quantification of blood velocity in mouse carotid and pulmonary arteries by ECG-triggered 3D time-resolved magnetic resonance angiography. NMR Biomed. doi:10.1002/nbm.1365
34. Margaritondo G, Hwu Y, Je JH (2004) Synchrotron light in medical and materials science radiology. La Rivista del Nuovo Cimento 27(7):1–40
35. Hwu Y, Tsai WL, Chang HM, Yeh HI, Hsu PC, Yang YC, Su YT, Tsai HL, Chow GM, Ho PC, Li SC, Moser HO, Yang P, Seol SK, Kim CC, Je JH, Stefanekova E, Groso A, Margaritondo G (2004) Imaging cells in tissues with refractive index radiology. Biophys J 87:4180–4187
36. Tamaki M, Kidoguchi K, Mizobe T, Koyama J, Kondoh T, Sakurai T, Kohmura E, Yokono K, Umetani K (2006) Carotid artery occlusion and collateral circulation in C57Black/6 J mice detected by synchrotron radiation microangiography. Kobe J Med Sci 52:111–118
37. Myojin K, Taguchi A, Umetani K, Fukushima K, Nishiura N, Matsuyama T, Kimura H, Stern DM, Imai Y, Mori H (2007) Visualization of intracerebral arteries by synchrotron radiation microangiography. Am J Neuroradiol 28:953–957
38. Akishima S, Matsushita S, Sato F, Hyodo K, Imazuru T, Enomoto Y, Noma M, Hiramatsu Y, Shigeta O, Sakakibara Y (2007) Cigarette-smoke-induced vasoconstriction of peripheral arteries: evaluation by synchrotron radiation microangiography. Circ J 71:418–422
39. Kuwabara E, Furuyama F, Ito K, Tanaka E, Hattan N, Fujikura H, Kimura K, Goto T, Hayashi T, Taira H, Shinozaki Y, Umetani K, Hyodo K, Tanioka K, Mochizuki R, Kawai T, Koide S, Mori H (2002) Inhomogeneous vasodilatory responses of rat tail arteries to heat stress: evaluation by synchrotron radiation microangiography. Jpn J Physiol 52:403–408
40. Kim JW, Seo HS, Hwu Y, Je JH, Kim A, Oh CW, Suh SY, Rha SW, Park CG, Oh DJ (2007) In vivo real-time vessel imaging and ex vivo 3D reconstruction of atherosclerotic plaque in apolipoprotein E-knockout mice using synchrotron radiation microscopy. Int J Cardiol 114:166–171
41. Hwu Y, Je JH, Margaritondo G (2005) Real-time radiology in the microscale. Nucl Instrum Meth A 551:108–118
42. Wang Y, Liu X, Im KS, Lee WK, Wang J, Fezzaa K, Hung DLS, Winkelman JR (2008) Ultrafast X-ray study of dense-liquid-jet flow dynamics using structure-tracking velocimetry. Nat Phys 4:305–309
43. Wang CH, Liu CJ, Wang CL, Hua TE, Obliosca JM, Lee KH, Hwu Y, Yang CS, Liu RS, Lin HM, Je JH, Margaritondo G (2008) Optimizing the size and surface properties of polyethylene glycol (PEG)-gold nanoparticles by intense X-ray irradiation. J Phys D 41:195301
44. Liu CJ, Wang CH, Chen ST, Chen HH, Leng WH, Chien CC, Wang CL, Kempson IM, Hwu Y, Lai TC, Hsiao M, Yang CS, Chen YJ, Margaritondo G (2010) Enhancement of cell radiation sensitivity by pegylated gold nanoparticles. Phys Med Biol 55:931–945
45. Goel R, Shah N, Visaria R, Paciotti GF, Bischof JC (2009) Biodistribution of TNF-α-coated gold nanoparticles in an in vivo model system. Nanomedicine 4:401–410
46. Prabaharan M, Grailer JJ, Pilla S, Steeber DA, Gong S (2009) Gold nanoparticles with a monolayer of doxorubicin-conjugated amphiphilic block copolymer for tumor-targeted drug delivery. Biomaterials 30:6065–6075
47. Lawrence MJ, Rees GD (2000) Microemulsion-based media as novel drug delivery systems. Adv Drug Deliv Rev 45:89–121
48. Song YF, Chang CH, Liu CY, Chang SH, Jeng US, Lai YH, Liu DG, Chung SC, Tsang KL, Yin GC, Lee JF, Sheu HS, Tang MT, Hwang CS, Hwu Y, Liang KS (2007) X-ray beamlines for structural studies at the NSRRC superconducting wavelength shifter. J Synchrotron Rad 14:320–325
49. Yang YC, Wang CH, Hwu YK, Je JH (2006) Synchrotron X-ray synthesis of colloidal gold particles for drug delivery. Mater Chem Phys 100:72–76
50. Wang CH, Hua TE, Chien CC, Yu YL, Yang TY, Liu CJ, Leng WH, Hwu Y, Yang YC, Kim CC, Je JH, Chen CH, Lin HM, Margaritondo G (2007) Aqueous gold nanosols stabilized by electrostatic protection generated by X-ray irradiation assisted radical reduction. Mater Chem Phys 106:323–329
51. Wang CH, Liu CJ, Wang CL, Hua TE, Obliosca JM, Lee KH, Hwu Y, Yang CS, Liu RS, Lin HM, Je JH, Margaritondo G (2008) Optimizing the size and surface properties of polyethylene glycol (PEG)–gold nanoparticles by intense X-ray irradiation. J Phys D 41:195301
52. Cai QY, Kim SH, Choi KS, Kim SY, Byun SJ, Kim KW, Park SH, Juhng SK, Yoon KH (2007) Colloidal gold nanoparticles as a blood-pool contrast agent for X-ray computed tomography in mice. Invest Radiol 42:797–806
53. Sharma P, Brown S, Walter G, Santra S, Moudgil B (2006) Nanoparticles for bioimaging. Adv Colloid Interfac 123:471–485
54. Brigger I, Dubernet C, Couvreur P (2002) Nanoparticles in cancer therapy and diagnosis. Adv Drug Deliv Rev 54:631–651
55. Hainfeld JF, Slatkin DN, Smilowitz HM (2004) The use of gold nanoparticles to enhance radiotherapy in mice. Phys Med Biol 49: N309–N315
56. Liu CJ, Wang CH, Chien CC, Yang TY, Chen ST, Leng WH, Lee CF, Lee KH, Hwu Y, Lee YC, Cheng CL, Yang CS, Chen YJ, Je JH, Margaritondo G (2008) Enhanced X-ray irradiation-induced cancer cell damage by gold nanoparticles treated by a new synthesis method of polyethylene glycol modification. Nanotechnology 19:295104
57. Morel AL, Nikitenko SI, Gionnet K, Wattiaux A, Lai-Kee-Him J, Labrugere C, Chevalier B, Deleris G, Petibois C, Brisson A, Simonoff M (2008) Sonochemical approach to the synthesis of $Fe_3O_4{\cdot}SiO_2$ core shell nanoparticles with tunable properties. ACS Nano 2:847–856
58. Ankamwar B, Lai TC, Huang JH, Liu RS, Hsiao M, Chen CH, Hwu YK (2010) Biocompatibility of Fe_3O_4 nanoparticles evaluated by in vitro cytotoxicity assays using normal, glia and breast cancer cells. Nanotechnology 21:075102
59. Huang FK, Chen WC, Lai SF, Liu CJ, Wang CL, Wang CH, Chen HH, Hua TE, Cheng YY, Wu MK, Hwu Y, Yang CS, Margaritondo G (2010) Enhancement of irradiation effects on cancer cells by cross-linked dextran-coated iron oxide (CLIO) nanoparticles. Phys Med Biol 55:469–482